NMR facilities were provided by the National Science Foundation (NSF Grant CHE 79-16100).

Registry No. I, 82292-83-9; II, 88271-76-5; III, 88271-77-6; IV, 88271-78-7; Va, 88271-79-8; Vb, 88271-83-4; Vc, 88271-81-2; VIa, 88271-80-1; VIb, 88271-84-5; VIc, 88271-82-3; $(\mu\text{-H})(\mu\text{-Cl})Re_2(CO)_6$(dppm), 88271-85-6; $(\mu\text{-Cl})_2Re_2(CO)_6$(dppm), 88271-86-7; $(\mu\text{-H})(\mu\text{-Cl})Re_2(CO)_6$(dmpm), 88271-87-8; $(\mu\text{-Cl})_2Re_2(CO)_6$(dmpm), 88271-88-9; $Re_2(CO)_{10}$, 14285-68-8; Re, 7440-15-5; $(\mu\text{-H})(\mu\text{-CH=}C_4H_9)Re_2(CO)_8$, 88294-19-3; 1-hexene, 592-41-6.

Supplementary Material Available: Thermal parameters (Table V), calculated hydrogen atom positions (Table VI), distances and angles associated with the phenyl groups (Table VII), crystal shape data (Table VIII), and observed and calculated structure factor amplitudes (Table IX) (61 pages). Ordering information is given on any current masthead page.

Paramagnetic Organometallic Molecules. 17.[1] Redox Chemistry of Homo- and Heteronuclear Carbon-, Germanium-, or Phosphorus-Capped Trimetal Clusters

Phillip N. Lindsay, Barrie M. Peake, Brian H. Robinson,* and Jim Simpson*

Department of Chemistry, University of Otago, Dunedin, New Zealand

Ute Honrath and Heinrich Vahrenkamp*

Institut für Anorganische Chemie der Universität, Freiburg, FRG

Alan M. Bond*

Division of Chemical and Physical Sciences, Deakin University, Waurn Ponds, Victoria, 3217 Australia

Received October 12, 1983

The redox chemistry of a series of capped tetrahedral clusters has been investigated by electrochemical and spectral techniques. Both homonuclear $RECo_3$ (R = Me, Ph, E = Ge, P) and heteronuclear $RECo_2M$ (R = Me, Ph, E = C, Ge, M = Cr, Mo, W; R = Me, Ph, E = P, M = Fe) and RPCoMM′ (R = Me, Ph, M = Fe, M′ = Mo, Ni) clusters are represented. The diamagnetic homonuclear cobalt clusters all undergo an electrochemically and chemically reversible one-electron reduction to the respective radical anions, and these were characterized by an analysis of their isotropic and anisotropic ESR spectra. Incorporation of another metal induces kinetic instability, and the redox behavior is a function of the capping group and the number of disparate metal atoms. Radical anions of the RECoMM′ clusters give paramagnetic fragmentation products under all conditions. The electrochemical behavior displayed by $RCCo_2M$ clusters is unusual in that an electrochemically and chemically irreversible process is followed by a chemically reversible step; possible interpretations of these data are given. Oxidation of the paramagnetic cluster $RPCo_3(CO)_9$ is chemically reversible, but attempts to isolate the cation were unsuccessful. Electrochemical and spectral parameters (IR, electronic, ESR) for this series of clusters and other capped trimetal clusters are compared and correlated with steric and electronic requirements of the metal and capping atoms.

Earlier papers in this series have dealt with the redox chemistry of the capped clusters CCo_3,[2,3] SCo_3,[4] SCo_2Fe,[4] and C_2Co_2.[5] Clusters of this type, in common with all neutral transition-metal carbonyl clusters of three or four nuclearity, characteristically undergo a one-electron reduction to a radical anion where the additional electron occupies an antibonding orbital centered on the metallic fragment.[2,4,6] These radical anions are activated to nucleophilic substitution, and electron-induced reactions offer a rapid and efficient synthesis of cluster derivatives.[7] However, the radical anions have varying degrees of thermodynamic and kinetic stability. The rate of decay is a function of metal–metal "bond strength", carbonyl configuration around the cluster, ion-pair formation or cation–anion association, and temperature.[8,9] A detailed ESR study of $SCo_2Fe(CO)_9$ indicated[4] that in a heteronuclear cluster the unpaired electron density is unequally distributed over the metallic unit although the radical anion has a reasonably long half-life.

The recent systematic synthesis of a variety of trinuclear clusters $ECo_3(CO)_9$ (I, E = RSi, RGe),[10] $ECo_2M'(CO)_8(Cp)$ (II, E = RC, RGe, M′ = Cr, Mo, W),[11] $RPCo_2Fe(CO)_9$,[12] and $EFeCoMo(CO)_8(Cp)$ (III,[13] E = RP, S), presented an opportunity to ascertain whether the generalizations formulated above were applicable to clusters with capping groups other than carbon or sulfur and to heteronuclear

(1) Part 16: Casagrande, L. V.; Taicheng, C.; Rieger, P. H.; Robinson, B. H.; Simpson, J.; Visco, S. J. *J. Am. Chem. Soc.*, in press.
(2) (a) Bond, A. M.; Peake, B. M.; Robinson, B. H.; Simpson, J.; Watson, D. J. *Inorg. Chem.* **1977**, *16*, 410. (b) Bond, A. M.; Dawson, P.; Peake, B. M.; Robinson, B. H.; Simpson, J. *Ibid.* **1979**, *18*, 1413.
(3) Peake, B. M.; Robinson, B. H.; Simpson, J.; Watson, D. J. *Inorg. Chem.* **1977**, *16*, 405.
(4) Peake, B. M.; Rieger, P. H.; Robinson, B. H.; Simpson, J. *Inorg. Chem.* **1981**, *20*, 2540.
(5) Peake, B. M.; Rieger, P. H.; Robinson, B. H.; Simpson, J. *J. Am. Chem. Soc.* **1980**, *102*, 156.
(6) (a) Strouse, C. E.; Dahl, L. F. *Discuss. Faraday Soc.* **1969**, *47*, 93. (b) Schilling, B. E. R.; Hoffmann, R. *J. Am. Chem. Soc.* **1979**, *101*, 3456.
(7) Arewgoda, M.; Robinson, B. H.; Simpson, J. *J. Am. Chem. Soc.* **1983**, *105*, 1893 and references therein.
(8) Kirk, C. M.; Peake, B. M.; Robinson, B. H.; Simpson, J. *Aust. J. Chem.* **1983**, *36*, 441.
(9) Lindsay, P. N. Ph.D. Thesis, University of Otago, 1982.
(10) Gusbeth, P.; Vahrenkamp, H. *Chem. Ber.* **1983**, *116*, in press.
(11) (a) Beurich, H.; Vahrenkamp, H. *Chem. Ber.* **1982**, *115*, 2385. (b) Richter, F.; Beurich, H.; Vahrenkamp, H. *J. Organomet. Chem.* **1979**, *166*, C5.
(12) Müller, M.; Vahrenkamp, H. *Chem. Ber.* **1983**, *116*, 2311.
(13) (a) Müller, M.; Vahrenkamp, H. *Chem. Ber.* **1983**, *116*, 2322, 2748. (b) Beurich, H.; Blumhofer, R.; Vahrenkamp, H. *Ibid.* **1982**, *115*, 2409.

0276-7333/84/2303-0413$01.50/0

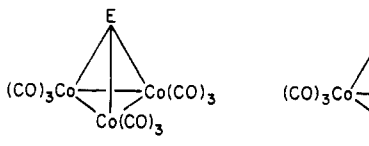

I

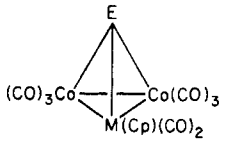

II

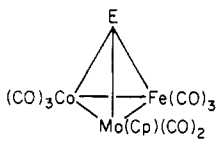

III

tetrahedral clusters. This paper is concerned with the detailed redox chemistry of these compounds. To simplify discussion, each cluster will be designated by a core description; e.g., $PhCCo_2Mo(CO)_8Cp \equiv PhCCo_2Mo$.

Experimental Section

Reagents. The compounds were prepared as described in other papers.[10-13] Before each electrochemical or ESR measurement the purity was checked by TLC and infrared spectra and, where possible, mass spectra. Tetrahydrofuran was dried with $CaCl_2$, distilled, and redistilled from sodium benzophenone ketyl immediately before use in vessels protected from light. Dichloromethane was distilled from CaH_2 under argon and stored over molecular sieves in vacuo and in the dark; 1,2-dichloroethane was similarly distilled under argon.

Measurements. Polarography and cyclic voltammetry studies were carried out with a PAR Model 174 analyzer driven by a PAR Model 175 programmer. Current–voltage curves were recorded on a Tektronix Model 5103 oscilloscope or an X-Y recorder. A conventional three-electrode cell was used in all experiments. The reference electrode was a Ag/AgCl (saturated LiCl, acetone) electrode isolated from the solution by a Vycor tip or, alternatively, a solid Ag/AgCl electrode immersed directly in the solution. These reference electrodes were calibrated before each run with a known[2] electrochemically and chemically reversible couple $[PhCCo_3(CO)_9]^{0,-}$ (DC polarographic conditions) in the same solvent and under the same conditions as the test solution. The potential ($E_{1/2}$) of this couple is −0.38 V in acetone, −0.56 V in CH_2Cl_2, and −0.80 V in 1,2-dichloroethane (all with saturated LiCl, acetone, Ag/AgCl reference). Reduction potentials of metal carbonyl clusters are exceptionally solvent dependent. Scan rates were 10 or 20 mV s^{-1} for polarographic and 50 mV s^{-1} to 5 V s^{-1} for voltammetric measurements. In common with other work on clusters in nonaqueous solvents, the peak separation in the cyclic voltammograms was often larger than 59 mV for an apparently electrochemically reversible couple. The "expected" ΔE_p for a reversible one-electron couple was taken for the couple $[PhCCo_3(CO)_9]^{0,-}$ measured under the same conditions.

All electrochemical measurements were carried out under argon. In general, the clusters used in this work were more soluble and stable in chlorinated solvents than acetone. For this reason most potentials in the tables will refer to data from dichloromethane and are the mean from several runs. Internal consistency was achieved between results obtained at Otago and Freiburg. Freshly prepared solutions $\sim 1 \times 10^{-3}$ mol dm^{-3} in compound and 1×10^{-1} mol dm^{-3} (TEAP in acetone) or 7×10^{-2} mol dm^{-3} (TBAP in CH_2Cl_2 or 1,2-$C_2H_4Cl_2$) in supporting electrolyte were used. In a number of cases severe fouling of the Pt working electrode was experienced; this was cleaned by placing the electrode in 1 mol dm^{-3} perchloric acid and applying a potential of 2 V vs. Ag/AgCl. Supportive evidence for the number of electrons involved in a particular reduction step was obtained by comparing the diffusion currents of cluster and $PhCCo_3(CO)_9$ solutions of equal concentration measured under comparable conditions as well as the usual electrochemical criteria. Alternatively, coulometry was employed for the more stable compounds. Because it was known that the heterometal clusters, in particular chromium carbon-capped species, do ultimately decompose in solution and under a CO atmosphere (but not within the time scale of our experiments) especial care was taken to ensure that the electrochemical processes were not the result of fragmentation compounds or decomposition products. TLC and infrared spectra of the electrolyte solutions were taken before and after each run and compared with the known parameters.[14] The compounds were recovered where there was any doubt; in no case were other cluster species found. In a few instances ($RCCo_2M$ clusters) electrochemistry was carried out in vacuo in a specially designed cell.

ESR measurements were made by the techniques described earlier.[2] All spectra were recorded on rigorously degassed solutions under high vacuum. Most spectra were produced by in situ electrolysis in the ESR cavity at potentials close to the first reduction peak potentials obtained from the cyclic voltammograms. Control of these potentials was not good with the low-temperature cell previously described,[2] but this did not pose problems for the homonuclear clusters as the potentials for the subsequent electrode processes were normally ~0.7 V more negative than the first. For the $RGeCo_2Mo$ and $RCCo_2M$ clusters, where the first and second potentials are close, a specially designed cell was constructed[15] in which simultaneous transient electrochemistry and reduction could be carried out. The quoted results were all reproducible over at least three different runs. The solution concentrations in all electrolytic reductions were approximately the same as for the electrochemical measurements. Most clusters used in this work fragmented rapidly when the reducing agent was Na/THF or Na/DME, and radical anions cannot be confidently generated in this manner.

Results

Electrochemistry and ESR of $RGeCo_3$. Polarographic and voltammetric data are given in Table I. In CH_2Cl_2 the current–voltage response for both clusters on Hg or Pt is characteristic of an electrochemically and chemically reversible one-electron transfer with production of a stable product; i.e., a plot of E vs. log $(i_d - i)/i$ slope 59 mV, $i_p(V)^{-1/2}$ and E_p^{red} independent of scan rate, and $i_p^{ox}/i_p^{red} \approx 1$ (where i_p^{ox} and i_p^{red} are the peak anodic and cathodic currents, E_p^{ox} and E_p^{red} are the anodic and cathodic peak potentials, and V is the scan rate). The same behavior is found in acetone.

Other irreversible electrode processes, similar to those found with $RCCo_3$ clusters,[2] were found at more negative potentials or on the anodic scan of the cyclic voltammograms if the switching potentials were >−1.20 V. Those at −1.15 (R = Ph) and −1.05 V (R = Me) are assigned to the irreversible formation of the dianion $RGeCo_3^{2-}$ (eq 1).

$$RGeCo_3 \overset{e}{\rightleftharpoons} RGeCo_3^{-}\cdot \rightarrow ReGeCo_3^{2-} \xrightarrow{\text{fast}} \text{decomposition} \quad (1)$$

No oxidation waves were seen. In all respects the electrochemical behavior of these germanium-capped clusters parallels that of the $RCCo_3$ compounds with $E_{1/2}(RGeCo_3) > E_{1/2}(RCCo_3)$. The magnitude of this difference in $E_{1/2}$ is solvent dependent; thus, it is 0.10 V in acetone, 0.08 V in CH_2Cl_2, and 0.24 V in 1,2-dichloroethane. This curious observation is due we believe to cation–anion association effects,[8] rather than specific changes in the solvation sheath, which are highlighted because electron transfer form the electrode is via the axial carbonyl groups of the cluster. There is a small substituent effect with the $E_{1/2}$ being more negative with an electron donor apical methyl group.

In situ electrochemical reduction of $RGeCo_3$ in CH_2Cl_2 in the ESR cavity, or external sodium reduction in THF at 293 K, produced a 22-line spectrum consistent with coupling of the unpaired electron in $RGeCo_3^{-}\cdot$ with three equivalent cobalt nuclei ($I = {}^7/_2$). Isotropic parameters (Table II) were derived from the typically asymmetric

(14) Beurich, H. G. Dissertation zur Erlangung der Doktorwürcle, Freiburg, 1980.
(15) Fernando, R.; McQuillan, A. J.; Peake, B. M., unpublished design.

Table I. Electrochemical Data for Trimetal Clusters[a]

cluster			mercury[b]			platinum[c]		
R	E	M_3	$E_{1/2}$, V	$E_{1/4} - E_{3/4}$, mV	n[d]	E_p,[c] V	ΔE_p, mV	$i_p{}^a/i_p{}^c$
Me	C	Co_3	−0.58	58	1	−0.61	70	1.0
			−1.37	92	...	−1.44	...	irrev
Ph	C	Co_3	−0.56	59	1	−0.60	65	1.0
			−1.29	80	...	−1.42	...	irrev
Me	Ge	Co_3	−0.32	59	1	−0.36	80	1.0
			−0.66	119	...	−1.18	...	irrev
Ph	Ge	Co_3	−0.31	62	1	−0.36	85	1.0
			−0.66	139	...	−1.27	...	irrev
Me	C	Co_2Cr	−0.76	44	(1)	−0.87	...	irrev
			−1.22	58	1	−1.24	86	0.88
Ph	C	Co_2Cr	−0.74	48	(1)	−0.85	...	irrev
			−1.18	58	1	−1.20	80	1.0
Me	C	Co_2Mo	−0.88	56	(1)	−0.86	...	irrev
			−1.19	65	1	−1.20	87	0.98
Ph	C	Co_2Mo	−0.80	54	(1)	−0.90	...	irrev
			−1.12	60	1	−1.16	80	1.0
Me	C	Co_2W	−0.87	52	(1)	...	...	irrev
			−1.19	62	1		84	0.97
Ph	C	Co_2W	−0.85	54	(1)	−0.98	...	
			−1.15	60	1	−1.28	95	1.0
Me	Ge	Co_2Mo	−0.56	54	1	−0.61	100	1.0
			−0.90	...	...	−1.12	...	irrev
Ph	Ge	Co_2Mo	−0.60	60	1	−0.68	140	1.0
Me	P	Co_2Fe	−0.58	64	1	−0.62	120	0.98
			...	..	...	...	...	...
Ph	P	Co_2Fe	−0.54	60	1		60	0.99
			−0.94	...	...		...	irrev
Bu	P	Co_2Fe	−0.57	59	1	...	72	1.0
Et_2N	P	Co_2Fe	−0.59	61	1	...	75	0.98
Me	P	CoFeMo	−1.13	65	1		210	>1
Ph	P	CoFeMo	−1.09	60	1		238	>1
t-Bu	P	CoFeMo	−1.11	61	1		217	>1
t-Bu	P	CoFeNi	−1.15	62	1		208	>1
Ph	P	Co_3	0.45	60	1	0.61	270	1.0

[a] In CH_2Cl_2; TBAP = 0.08 × 10^{-1} M, compound ≈ 10^{-3} M. Potential in V vs. Ag/AgCl; 293 K. [b] Scan rate 20 mV s^{-1}, drop time 0.5 s. [c] Scan rate 200 mV s^{-1}. [d] Determined by coulometry and/or normal electrochemical response criteria. Values in parentheses indicate that the reduction step is one electron but the response at 293 K does not electrochemically correspond to one (see text).

spectrum by the methods outlined earlier[16] using the line width parameters $\tau_R = 5.45 \times 10^{-11}$ s and $\alpha' = 0.50$ mT for computer simulations. These parameters gave a good match between experimental and simulated spectra, and there was no evidence to suggest hyperfine coupling to the germanium capping atom ($I = {}^9/_2$, 7.76% abundance). The lifetimes of these radical anions are at least comparable to that of the long-lived $[PhCCo_3(CO)_9]^{-}\cdot$.[2]

ESR spectra of frozen THF solutions of $RGeCo_3^{-}\cdot$ were obtained at 133 K. The spectra clearly indicate one large hyperfine tensor component, identified with the well-resolved 22 parallel features. Analysis with small second-order corrections gave the values of $g_\parallel$ and $a_\parallel$ in Table II. Perpendicular features were unresolved due to the large line widths, but it is reasonable to assume that the other hyperfine components are small and are given by the expression $a_\perp = (3\langle a\rangle - a_\parallel)/2$. These are the values given in Table II assuming negative isotropic coupling constants. The parallel tensor components are smaller in comparison with carbon- and sulfur-capped analogues,[4] which results in the smaller isotropic hyperfine coupling constants. The tensor components are in fact similar to those of the heteronuclear $SFeCo_2^{-}\cdot$ where 60% of the spin density resides on the two cobalt atoms.[4] From MO arguments (see ref 4) the LUMO is expected to be of $a_2{}^*(d_{xy})$ character.[4,5] The dipolar hyperfine tensor is computed (from $b = a - \langle a\rangle$) to be (assuming negligible spin–orbit coupling): R = Me, $b_\parallel = -2.87$ mT and $b_\perp = 1.43$ mT; R = Ph, $b_\parallel = -3.49$ mT and $b_\perp = 1.09$ mT. The negative value is consistent with $a_2{}^*(d_{xy})$ character.[5] Now $b_\parallel = -{}^4/_7 P\,\rho^{3d}$, where $P = 30.2$ mT, which gives a cobalt 3d spin density of $\rho^{3d} = 0.17$ and 0.20 for the $[MeGeCo_3]^{-}\cdot$ and $[PhGeCo_3]^{-}\cdot$ anions, respectively. These values for ρ^{3d} are indeed lower than that for $SFeCo_2(CO)_9^{-}\cdot$ (0.29) as well as $CCo_3^{-}\cdot$ (~0.25) and SCo_3 (0.25). Possible reasons for this will be discussed later.

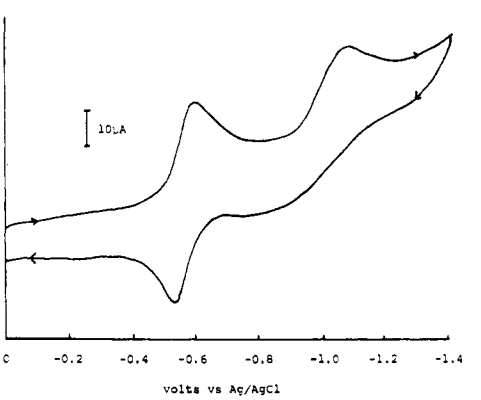

Figure 1. Cyclic voltammogram of $MeGeCo_2Mo(CO)_8Cp$ in acetone (0.1 M TEAP) on Pt (scan rate 100 mV s^{-1}; 293 K).

$RGeCo_2Mo$ (R = Me, Ph). Direct current (dc) polarograms and cyclic voltammograms of $RGeCo_2Mo$ in CH_2Cl_2 show two reduction waves (Figure 1). The first

(16) Peake, B. M.; Rieger, P. H.; Robinson, B. H.; Simpson, J. *Inorg. Chem.* **1979**, *18*, 1000.

Table II. ESR Data for Paramagnetic Species from the Reduction of Trimetal Clusters[a]

cluster			radical anions[b]						
			⟨g⟩	$g_\parallel$	$g_\perp$	⟨a⟩	$a_\parallel$	$a_\perp$	$b_\parallel$[g]
Me	C	Co_3[c,d]	2.011	2.000	2.020	−3.66	−7.58	−1.60	
Ph	C	Co_3[c,d]	2.013	1.996	2.022	−3.58	−7.90	−1.42	−4.32
Me	Ge	Co_3[c]	2.029	2.009	2.000	−3.15	−6.02	−1.72	−2.87
Ph	Ge	Co_3[c]	2.031	2.036	2.027	−3.16	−6.65	−1.42	−3.49
Me	C	Co_2Mo[f]	2.012	2.010	2.008	−3.34	−6.61	−1.71	−3.24
Ph	C	Co_2Mo[f]	2.007	2.014	2.003	−3.35	−6.63	−1.71	−3.24
Ph	C	Co_2W	2.022	2.002	2.032	−3.59	−5.57	−2.60	−1.98
Me	Ge	Co_2Mo[c]	2.010	2.015	2.007	−3.16	−6.68	−1.40	−3.52
Ph	Ge	Co_2Mo[c]	2.024	2.015	1.980	−3.04	−6.61	−1.24	−3.57
Me	P	Co_2Fe	2.020	2.019	2.021	−2.85	−6.86	−0.85	−4.01
Ph	P	Co_2Fe	2.030	2.019	2.035	−2.89	−6.87	−0.90	−3.98
Ph	P	Co_3	2.033	2.032	2.030	−3.25	−7.47	−1.14	−4.22
	S	Co_2Fe[c,e]	2.015	2.017	2.014	−3.4	−6.6	−1.8	−3.2

cluster			other species
Ph	C	Co_2Cr[f]	eight-line spectrum at −40 °C; ⟨g⟩ = 2.038, ⟨a⟩ = −4.05
Ph	C	Co_2Mo[f]	asymmetric eight-line spectrum at 20 °C; ⟨a⟩ = −4.8
Me	C	Co_2Mo[f]	>eight-line symmetrical spectrum at −50 °C; ⟨g⟩ = 2.012, ⟨a⟩ = −3.34; asymmetric eight-line spectrum at 20 °C; ⟨a⟩ = −4.80
Ph	C	Co_2W	asymmetric eight-line spectrum 0 → −60 °C; ⟨a⟩ = −4.90
Ph	P	CoFeMo	doublet at 20 °C; g = 2.033; asymmetric eight-line spectrum at −60 °C; ⟨a⟩ = 6.0; broad single resonance in frozen solution spectrum
Me	P	CoFeMo	doublet at 20 °C; g = 2.036; after some time fifteen-line spectrum as for $MePCo_2Fe^{-}\cdot$ builds up; nothing observed at low temperatures.
t-Bu	P	CoFeNi	asymmetric eight-line spectrum at −60 °C; ⟨g⟩ = 2.049, ⟨a⟩ = −2.21; frozen solution; two sets of resonances; most prominent has $g_\parallel$ = 2.097 and $a_\parallel$ = −4.89.

[a] Produced by in situ electrolysis in ESR cavity in CH_2Cl_2 unless stated otherwise; hyperfine coupling constants in mT. [b] Parallel and perpendicular features from an analysis of the frozen solution spectra; isotropic values from spectra recorded at −60 °C. This is little temperature variation in the isotropic parameters. [c] The same spectra were obtained by reducing the cluster with Na in THF. [d] Reference 16. [e] Reference 4. [f] In THF. [g] Calculated assuming axial symmetry.

wave has the characteristics of a reversible one-electron transfer with the formation of a soluble stable radical anion (E vs. log $(i_d - i)/i \approx 60$ mV, $i_p^c(V)^{-1/2}$ and E_p^c independent of scan rate, and $i_p^a/i_p^c \approx 1$). The second reduction wave, at 0.34 V more negative potential, has a dc polarographic limiting current slightly larger than that for the first wave, but under conditions of cyclic voltammetry the process is chemically irreversible.[17] The second process has the characteristics of an ECE mechanism. Although the separation between the first and second reduction processes is small, relative to other clusters, an assignment of the second couple to the second reduction step is not unreasonable (eq 2).

$$RGeCo_2Mo + e \rightleftharpoons [RGeCo_2Mo]^{-}\cdot \xrightarrow{e} [RGeCo_2Mo]^{2-} \quad (2)$$

Well-resolved isotropic and anisotropic ESR spectra of the radical anions $RGeCo_2Mo^{-}\cdot$ were obtained by in situ electrolysis at −0.55 V in CH_2Cl_2.[18] The isotropic g values and cobalt hyperfine coupling constants are given in Table II and were independent of temperature. The frozen solution spectra were analyzed in terms of two equivalent cobalt nuclei, two hyperfine tensor components being accessible from the spectra[5] (Figure 2). Prominent, equally spaced, features correspond to the largest hyperfine tensor component arising from parallel or colinear principal axes for the two cobalt nuclei. Other features in the spectra are associated with another set of 15 lines that correspond to the second largest hyperfine tensor component. This component corresponds to principal tensor axes that are not parallel for the two cobalt nuclei, and the line function and spacings are a function of the angle α between the principal axes of the hyperfine tensors.[5] A detailed analysis of this and similar ESR spectra will be given elsewhere.[19]

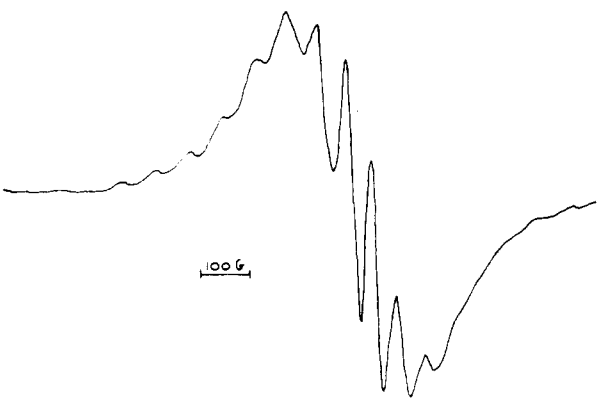

Figure 2. Frozen solution ESR spectrum of $MeGeCo_2Mo(CO)_8Cp$ in THF.

$RCCo_2M$ [R = Me, Ph, M = $Cr(CO)_2Cp$, $Mo(CO)_2Cp$, $W(CO)_2Cp$]. The redox chemistry of the carbon-capped heteronuclear clusters provided an interesting contrast to the germanium analogues just described. Their electrochemical behavior is extraordinarily complex, and it will be convenient to deal with each cluster individually. The data demonstrate that the electrochemical response is kinetically controlled and is a function of heteroatom, CO, solvent, and temperature. In view of the bewildering variety of electrochemical responses, it should be emphasized that chemical and spectroscopic analysis of the solutions before electrochemical or ESR experiments confirmed that

(17) See: Midholova, D; Fiedler, J.; Vlcek, A. A. *J. Electroanal. Chem. Interfacial Electrochem.* **1983**, *143*, 195 for a discussion of the kinetic control exerted by conproportionation or disproportionation reactions on the electrochemical response associated with the first and second reduction steps.

(18) Identical spectra were obtained in THF.

(19) Peake, B. M.; Robinson, B. H.; Simpson, J.; Vahrenkamp, H., manuscript in preparation.

Table III. Electrochemical Data for $RCCo_2M$ Clusters[a]

conditns (temp)	$E_{1/2}$(C)	$E_{1/2}$(D)	i_d(D)/i_d(C)	E_p^c(C)	E_p^c(D)	i_p^c(D)/i_p^c(C)	E_p^c(C)	E_p^c(D)	i_p^c(D)/i_p^c(C)
				$MeCCo_2Cr(CO)_8Cp$					
Ar (293)	−0.58	−1.04	0.61	−0.65	−1.08 (−1.01)	0.76	*−0.69*	*−1.07 (0.98)*	*0.80*
CO (293)	−0.59	−1.03	0.08	−0.67	−1.07 (−0.99)	0.08	*−0.73*	*−1.07 (−1.00)*	*0.10*
Ar (253) (213)	−0.66	−1.02	0.80	−0.72	−1.03 (−0.97)	1.0	*−0.84*	*−1.06 (−0.99)*	*0.40*
				$PhCCo_2Mo(CO)_8Cp$					
Ar (293)	−0.62	−0.94	1.2	−0.72	−0.98 (−0.91)	1.10	*−0.72*	*−0.98 (−0.91)*	*1.1*
CO (293)	−0.70	−0.96	1.4	−0.77 (−0.63)	−1.00 (−0.92)	1.15	*−0.77 (−0.63)*	*−1.00 (−0.92)*	*0.85*
Ar (253) (213)	−0.76	−0.95	1.4	−0.79	− 0.95 (−0.89)	1.4	*(−0.60)*	*−1.00 (−0.90)*	
				$PhCCo_2W(CO)_8Cp$					
Ar (293)	−0.67	−0.97	1.07	−0.73	−1.01 (−0.93)	1.3	*−0.80*	*−1.07 (−0.99)*	*1.2*
CO (293)	−0.75	−0.98	1.10	−0.81 (−0.72)	−1.00 (−0.95)	1.0	*−0.84 (−0.7)*	*−0.98 (−0.91)*	*1.1*
Ar (253) (213)							*(−0.60)*	*−1.06 (−0.97)*	

[a] Potentials in V vs. Ag/AgCl in acetone (0.1 M TEAP); scan rate 20 mV s^{-1} (polarography) to 500 mV s^{-1} (cyclic voltammetry); drop time 0.5 s^{-1}. C and D refer to the first and second reduction steps (see text). Data in italics refer to Pt; all other data on Hg. Data in parentheses are the anodic peak potentials associated with a particular E_p^c(C) or E_p^c(D).

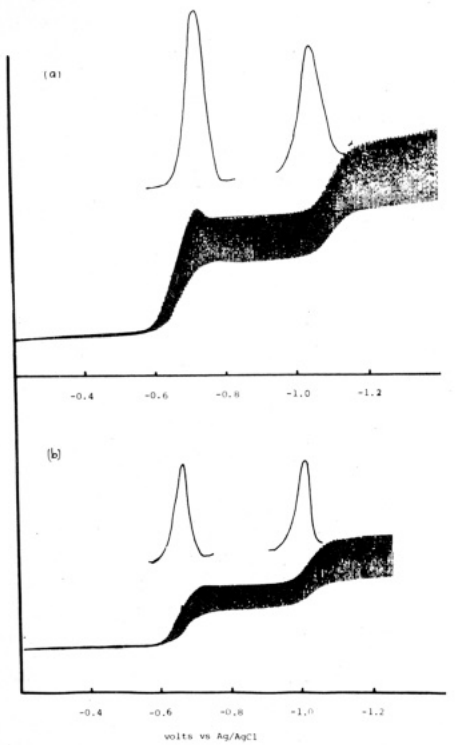

Figure 3. dc and differential pulse polarograms of $MeCCo_2Cr(CO)_8Cp$ in acetone (drop time 0.5 s; scan rate 10 mV s^{-1}): (a) 293 K; (b) 253 K.

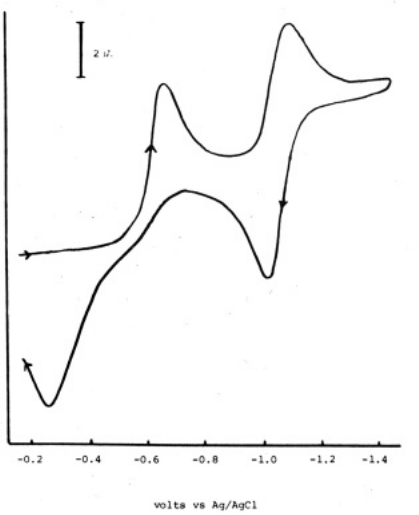

Figure 4. Cyclic voltammogram of $MeCCo_2Cr(CO)_8Cp$ in acetone (0.1 M TEAP) on Hg at 293 K (scan rate 500 mV s^{-1}).

pure samples were used and the work carried out at Otago and Freiburg was in complete agreement. Great care was taken to exclude oxygen. Controlled potential electrolysis in THF or CH_2Cl_2 at 293 K of any carbon-capped cluster at potentials slightly positive of the respective first reduction potential led to decomposition; the products were organic, inorganic, and metal carbonyl species which, apart from $Co(CO)_4^-$ and $CpM(CO)_3^-$, were not identified.

$MeCCo_2Cr$. Figure 3a shows a dc and differential pulse polarogram for this cluster in acetone.[20] Two reduction processes are evident at 293 K (Table I). The first, at −0.58 V, is considerably steeper than expected for a diffusion-controlled one-electron step ($E_{1/4} - E_{3/4}$ = 44 mV), and the data imply that an ECE mechanism is operative. The second step at −1.04 V has the characteristics of an electrochemically reversible process (see Table I). It is important to note that the limiting current for the sum of

(20) We will discuss the electrochemical responses in acetone in this section as this is the solvent referred to in the figures. The responses in CH_2Cl_2 and other chlorinated solvents were qualitatively similar, with an appropriate shift in potential as discussed in the experimental. However, the peak separation between the first and second reduction steps were generally smaller than in acetone, whereas the reverse held for the peak separation in THF. The first reduction step was also more prominent in THF; see the discussion on $PhCCo_2W$.

(21) DC polarograms of the $RCCo_2Cr$ clusters frequently displayed abnormal "humped" limiting currents at 293 K that are typical of strong adsorption or catalytic processes on Hg;[22] they were absent below 273 K.

(22) Bond, A. M. "Modern Polarographic Methods in Analytical Chemistry"; Marcel Dekker: New York, 1980.

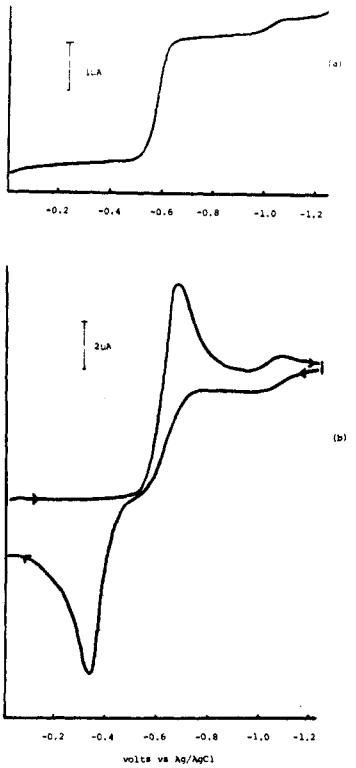

Figure 5. Electrochemical behavior of $MeCCo_2Cr(CO)_8Cp$ in acetone under an atmosphere of CO (0.1 M TEAP): (a) dc polarogram (drop time 0.5 s; scan rate 10 mV s^{-1}); (b) cyclic voltammogram on Hg (scan rate 500 mV s^{-1}).

these two reduction steps is close to twice that for the known one-electron reduction of $PhCCo_3(CO)_9$ in equimolar concentration, and thus an overall two-electron reduction occurs. However, the ratio of the limiting currents varies with drop time, concentration, and temperature (Table III), suggesting a nonunity order chemical process accompanies the charge-transfer process. A cyclic voltammogram on Hg (Figure 4) displays two waves of approximately equal height (each one-electron) corresponding effectively to the low-temperature dc polarogram shown in Figure 3b.

Thus under short-time scale conditions two one-electron reduction steps are observed. Figure 4 shows that the most positive reduction step remains chemically irreversible even though on this time scale the process is an apparently one-electron reduction. This implies that at least two chemical reactions contribute to the reduction step at −0.58 V. One leads to an ECE mechanism that is seen on long-time scales and the other faster chemical step to an EC mechanism. The overall process must be an ECCE, or even more complicated process. The more negative process remains chemically reversible under all conditions, but its current magnitude diminishes whenever the ECCE mechanism for the first step is important. An assignment for the small oxidation wave at −0.34 V is discussed below. With the assumption that the initial reduction product is the radical anion, then it must be a more reactive and unstable species than other capped cluster radical anions.

Figure 5a,b shows a dc polarogram and cyclic voltammogram on Hg in acetone at 293 K in the presence of CO. The first reduction step now becomes essentially a two-electron transfer. That is, the ECCE mechanism is enhanced in importance. Concomitantly, the second reduction step is drastically reduced in magnitude, as expected. There is a very well-defined peak at $E_p^{ox} = -0.34$ V that can be assigned to the known[3] radical anion $[MeCCo_3(CO)_9]^{-\cdot}$. This particular peak is almost absent

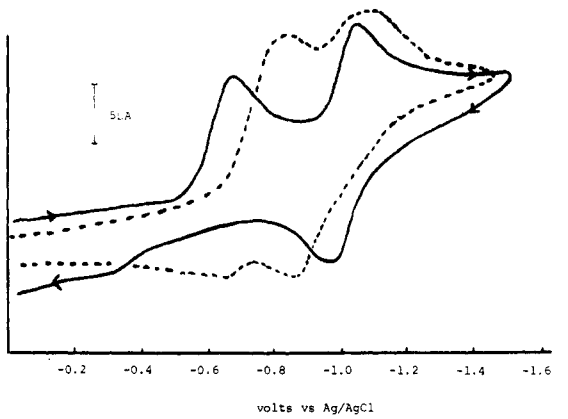

Figure 6. Cyclic voltammograms of $MeCCo_2Cr(CO)_8Cp$ on Pt in acetone (0.1 M TEAP; scan rate 500 mV s^{-1}): —, 293 K; - - -, 213 K.

at fast scan rates and low temperatures (see Figure 6) and is likely a decomposition product of the $MeCCo_2M^{-\cdot}$ radical anion (as is $Co(CO)_4^-$) since it is still present in scans switched before the second reduction step.

Cyclic voltammograms on Pt at 293 K resemble those on Hg. At 213 K on Pt (Figure 6) the two reduction processes become much closer together and the first process has some degree of chemical reversibility.[23] Furthermore, the second process is diminished in height as the first process becomes chemically reversible (Table III). These low-temperature data demonstrate that the reversible $E_{1/2}^r$ ($\simeq E^\circ$) value for the first electrode process is more negative than that for the $[MeCCo_3(CO)_9]^{0,-}$ couple but also that under other conditions the $E_{1/2}^r$ or E_p^{red} potentials are strongly influenced by coupled chemical reactions.

In view of the rapid chemical reactions that follow the reduction of the cluster it is not surprising that no paramagnetic species compatible with $MeCCo_2Cr^{-\cdot}$ were found in the ESR spectra. Prolonged in situ electrochemical reduction of the clusters in CH_2Cl_2 in the temperature range 213–293 K gave eight-line ESR spectra of marked asymmetry; the parameters are given in Table II. These asymmetric spectra and hyperfine coupling constant (which exhibits only a slight temperature dependence ($d\langle a\rangle/dT \approx -0.09$ mT K^{-1}) are compatible with a species in which the unpaired electron is associated with a single cobalt nucleus.[1] No coupling to Cr ($I = {}^3/_2$, 9.5%) was seen, although partial splitting of some high-field lines was discernible in the ESR spectrum. If a solution electrolyzed at 213 K was rapidly frozen, the eight-line spectrum disappeared but it was not replaced by the expected 15-line spectrum for $MeCCo_2Cr^{-\cdot}$ (cf. the Mo and W clusters vide infra).

$PhCCo_2Cr$. Compared to the methyl analogue the ECCE character of the first reduction step is enhanced and there is a considerable shift in the reduction potentials (Table I). This is probably a reflection of the kinetics rather than thermodynamics because at 213 K the cyclic voltammograms on Pt have similar characteristics to those of $MeCCo_2Cr$; CO dependence was the same as $MeCCo_2Cr$. Asymmetric eight-line species only were observed in the ESR spectra (Table II).

$PhCCo_2Mo$. Figure 7 shows the polarographic response for $PhCCo_2Mo$ at 293 K. Two one-electron reduction

(23) Data for cyclic voltammograms recorded at 2 or 5 V s^{-1} were comparable with those recorded at low temperatures and are not reproduced in the paper.

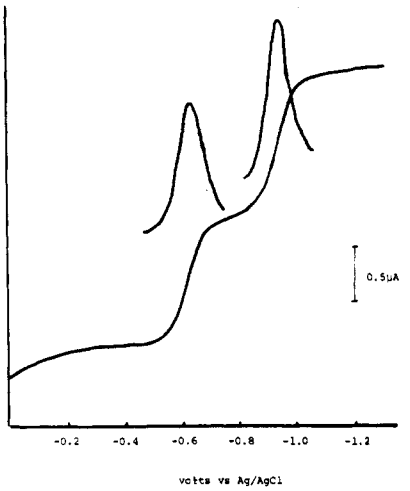

Figure 7. dc and differential pulse polarogram of $PhCCo_2Mo(CO)_8Cp$ in acetone (0.1 M TEAP; scan rate 10 mV s^{-1}; drop time 0.5 s^{-1}; 293 K).

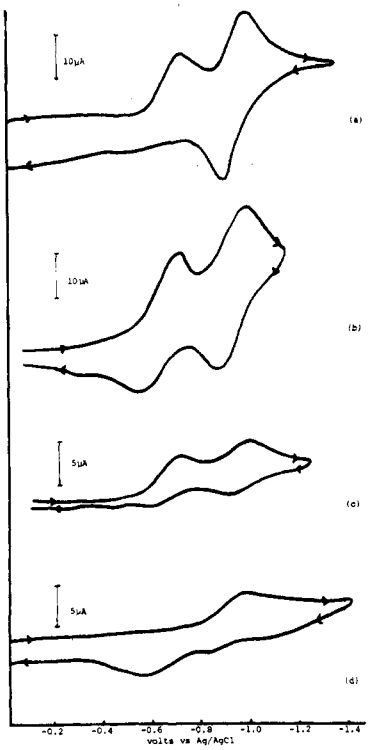

Figure 8. Cyclic voltammograms of $PhCCo_2Mo(CO)_8Cp$ on Pt in acetone (0.1 M TEAP): (a) scan rate 500 mV s^{-1}, 293 K under argon; (b) under CO, scan rate 500 mV s^{-1}, 293 K; (c) under CO, scan rate 100 mV s^{-1}, 293 K; (d) under argon, scan rate 500 mV s^{-1}, 213 K.

processes are seen (–0.62 and –0.94 V, respectively), and superficially this appears similar to the response for the $MeCCo_2Cr$ cluster at low temperatures (cf. Figure 3b). That is, no ECE mechanism is operative, and they have slopes consistent with electrochemically reversible processes.

In the presence of CO the two waves become much closer together (see Table III), but unlike the $RCCo_2Cr$ case the second reduction step does not decrease at the expense of the first. Companion cyclic voltammograms of $PhCCo_2Mo$ at Pt under N_2 and CO are shown in Figure 8a–c. Two one-electron steps are seen under N_2, with only the second being chemically reversible, whereas, under CO, the first step achieves a considerable degree of chemical reversibility at relatively fast scan rates. An oxidation wave at –0.38 V observed under CO can be assigned[2] to the oxidation of $[PhCCo_3(CO)_9]^{-}\cdot$. The substantial scan rate and temperature dependence are included in the data in Table III. Interestingly, the more negative process remains chemically reversible irrespective of whether the first step appears to be chemically reversible or irreversible, a fact which is of crucial importance in any mechanistic interpretation of these redox processes. At low temperatures only a *single reduction* step is seen but the intriguing feature (Figure 8d) is that there are *two* oxidation waves on the reverse scan, the most positive corresponding to the oxidation component of the first reduction step at room temperature. This, together with the non-integral peak current (~1.2 electrons), is a clear indication that the first reduction step involves an ECE process. Note also that there is only a slight shift in the potential of the second reduction step so effectively the peak current of the first step decreases and ultimately disappears at 213 K, which is different behavior to the chromium analogue (vide supra).

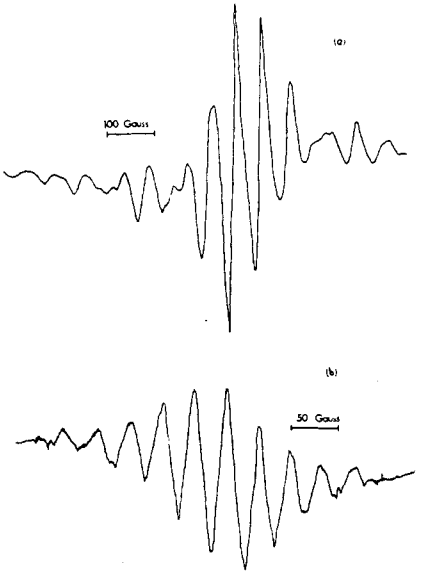

Figure 9. ESR spectrum of $MeCCo_2Mo(CO)_8Cp^{-}\cdot$ radical anion in THF: (a) frozen solution; (b) 213 K.

When the cluster $PhCCo_2Mo$ is reduced at –0.7 V vs. Ag/AgCl at 213 K in situ in an ESR cavity, a poorly defined spectrum of at least eight lines is observed. On freezing this solution a rather asymmetric anisotropic 15-line spectrum ($\langle a \rangle_{Co}$ = 3.34 mT) is produced that on rewarming to 213 K converts back to the initial spectrum.[24] The parameters for the anisotropic spectrum (Table II) are consistent with the formation of a radical anion $PhCCo_2Mo^{-}\cdot$, and the reversibility with temperature indicates that this radical anion has a reasonable lifetime. If the in situ electrochemical reduction is carried out at temperatures above 230 K, an asymmetric eight-line spectrum, $\langle a \rangle_{Co}$ = 4.8 mT, replaces the low-temperature spectrum. The data (Table II) are comparable with those found in other low-valent monocobalt carbonyl radical species.[1]

(24) Unpublished work[9] and ref 8 suggest that the lifetime and reactivity of cluster radical anions are influenced by the counterion. In particular, PPN^{+} is very effective in extending their lifetimes. An ESR spectrum produced in CH_2Cl_2 (0.08 M $PPN^{+}Cl^{-}$) at 213 K still exhibited an eight-line profile but with $\langle a \rangle$ = 3.5 mT and $\langle g \rangle$ = 2.009, parameters which are different to those with TBAP as electrolyte. Furthermore, there was evidence for another species with $\langle g \rangle$ = 1.956. However, the chemical reversibility of the first reduction step was better at 293 K and the cyclic voltammograms were similar to those under CO with $PPN^{+}Cl^{-}$ as supporting electrolyte.

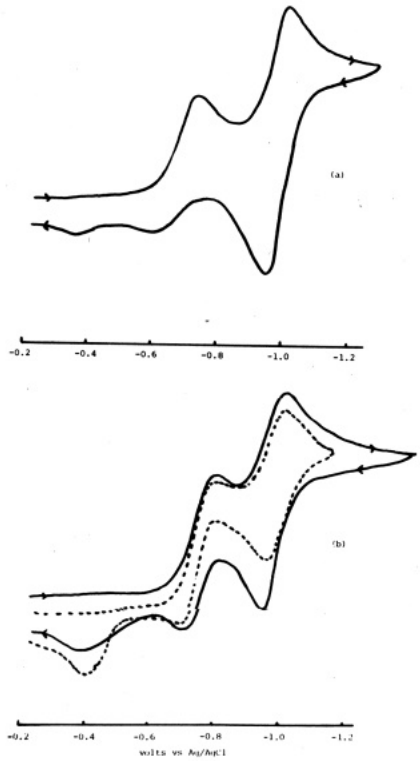

Figure 10. Cyclic voltammograms of $PhCCo_2W(CO)_8Cp$ on Hg at 288 K in acetone (0.1 M TEAP): (a) scan rate 500 mV s^{-1} under argon; (b) under CO, —, scan rate 500 mV s^{-1}, - - -, scan rate 200 mV s^{-1}.

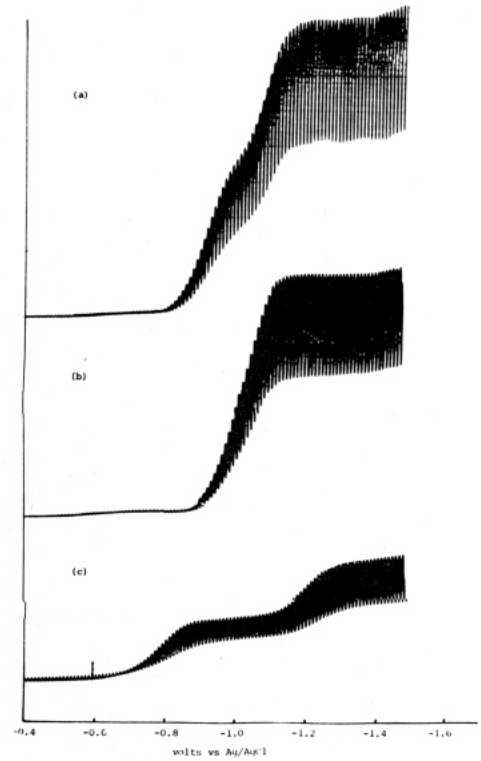

Figure 11. dc polarograms of $PhCCo_2W(CO)_8Cp$ (drop time 0.5 s^{-1} scan rate 10 mV s^{-1}): (a) CH_2Cl_2, 295 K; (b) CH_2Cl_2, 252 K; (c) THF, 293 K.

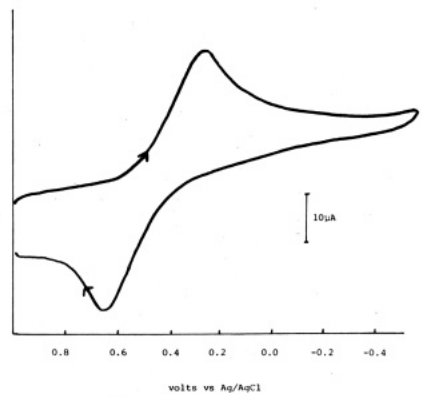

Figure 12. Cyclic voltammogram of $PhPCo_3(CO)_9$ in CH_2Cl_2 (0.08 M TBAP) at 293 K on Pt (scan rate 500 mV s^{-1}).

$MeCCo_2Mo$. Data for this cluster are summarized in Table I from which it can be seen that the essential electrochemical responses follow the pattern found in $PhCCo_2Mo$. This compound provided the best ESR spectrum of a carbon-capped radical anion (Figure 9) at low temperatures. Again the parameters for both the isotropic and anisotropic spectra are totally consistent with the assignment to $MeCCo_2Mo^{-}\cdot$. At room temperature the spectrum of $MeCCo_2Mo^{-}\cdot$ is superseded by an asymmetric eight-line spectrum similar to, but not identical with, that found with $PhCCo_2Mo$.

$PhCCo_2W$. In acetone two well-defined waves are observed in the dc polarograms irrespective of whether the scans were carried out under CO. Data are summarized in Table III. Under argon the two waves are of equal height (the slope of the first reduction step is greater than expected for a first-order diffusion-controlled process, whereas that for the second is consistent with an electrochemically reversible one-electron transfer), whereas the first wave is increased at the expense of the second by the addition of CO, and there is a concurrent shift of the first wave to more negative potentials, but the second potential is unchanged.

The substantial CO dependence is also seen in the cyclic voltammograms on Hg, and this fact, together with the relative dominance of the first reduction step in the presence of CO and the marked temperature variation (Figure 10), suggests that this system has a number of similar mechanistic features to the $RCCo_2Cr$ system. In the $PhCCo_2W$ case there is also a marked variation in electrochemical behavior with solvent. This is more clearly seen in the dc polarograms (Figure 11). In CH_2Cl_2, at 295 K, the two waves are distinct, whereas at 256 K they have merged to give an apparent two-electron wave. On the other hand, the two waves are clearly defined over all temperatures in THF. A marked solvent dependence of the reduction potential of metal carbonyl clusters has been noted previously,[25] but the shifts in this compound are more substantial and indicate that the donor ability of the solvent has an important role in the ECCE mechanism.

By carrying out an in situ electrolysis of $PhCCo_2W$ at 213 K and then freezing the THF solution, a weak ESR spectrum was obtained of at least 12 components. An analysis of this spectrum gave $g_{\parallel} = 2.002$, $a_{\parallel} = -5.58$ mT, and $a_{\perp} = -2.50$ mT, parameters which are compatible with a cluster radical anion (cf. those for $RCCo_2Mo^{-}\cdot$). Since both reduction processes achieve chemical reversibility at low temperatures and the performance of the ESR cell did not unambiguously define the electrolysis potential, it is not possible from our data to associate the ESR spectrum with either reduction step. Electrolysis at higher temperatures than 213 K gave an eight-line ESR spectrum with a coupling constant of $\langle a \rangle_{Co} = -4.90$ mT (Table II) typical of a monocobalt species,[1] i.e., of a fragmentation

(25) See: Colbran, S.; Robinson, B. H.; Simpson, J. *Organometallics* **1983**, *2*, 943.

product. No signal was observed at room temperatures.

$PhPCo_3$. Unlike the other clusters discussed in this paper this compound, isoelectronic with $SCo_3(CO)_9$, is a 19-electron species and inherently paramagnetic.[26] A reversible one-electron oxidation process (E vs. log $(i_d - i)/i$ = 60 mV, i_p^a/i_p^c = 1.04) on Hg and Pt at 293 K in CH_2Cl_2 can be confidently assigned to the formation of a cation, $PhPCo_3^+$. The reversibility of this process (Figure 12) indicates that the cation is chemically accessible but attempts to isolate the cation by Ag^+, I_2, or electrochemical oxidation were not successful. The first oxidation process is followed on Pt by a poorly defined irreversible step at E_p^a = 1.0 V, and there is an irreversible reduction wave at −0.84 V (eq 3).

$$PhPCo_3^{2+} \xrightarrow{e} PhPCo_3^{+} \rightleftharpoons PhPCo_3 \xrightarrow{e} PhPCo_3^{-}\cdot \text{ decomposition} \quad (3)$$

A well-resolved isotropic ESR spectrum of $PhPCo_3$ has been reported previously.[26] Analysis of the far from ideal frozen solution spectrum gave the parameters in Table II. Despite the 100% abundance of ^{31}P, $I = {}^1/_2$, no coupling to the phosphorus capping atom was resolved, and this is compatible with the odd electron residing in an a_2^* Co_3 orbital. The axially symmetric g and hyperfine tensors are very similar to those of $SCo_3(CO)_9$, showing that there is a comparable perturbation of the capping groups S and PhP on the upper bonding and a_2^* levels, and on the effective nuclear charge on the cobalt atoms.

$RPCo_2Fe$. Current–voltage curves at Pt or Hg in CH_2Cl_2 for these 18-electron clusters show a reversible one-electron process corresponding to the formation of a radical anion, $RPCo_2Fe^-\cdot$. $PhPCo_2Fe$ also gave a second irreversible reduction step at more negative potentials, but this was absent in $MePCo_2Fe$. The reduction of the clusters by a potassium mirror in DME, or electrochemically intra muros, gave the expected 15-line ESR spectrum[26] of $RPCo_2Fe^-\cdot$. The lifetime of this radical anion is considerably shorter than those of germanium- or carbon-capped species. It is interesting that the isotropic and anisotropic ESR parameters are overall lower than those for $RPCo_3^-\cdot$ and also the isoelectronic $SFeCo_2^-\cdot$. The reason for lower spin density on the cobalt atoms in $RPCo_2Fe^-\cdot$ compared to $SFeCo_2^-\cdot$ is not clear.

RPFeCoMo (R = Me, Ph, Et_2N) and *t*-BuPFeCoNi. These compounds represent some of the few examples of trimetallic clusters with three different metal components.[13] An interesting question arises as to where the extra electron in a radical anion will reside; unfortunately, the instability of the radical anions meant there was insufficient data to provide an answer.

All the RPFeCoMo clusters are reduced on Hg or Pt in CH_2Cl_2 at 293 K, but, although the diffusion currents suggest a one-electron process, the current–voltage responses (e.g., E_p is dependent on scan rate, small anodic current) show that the reduction is chemically and electrochemically irreversible, even at low temperatures. Irreversibility undoubtedly arises from a fast fragmentation reaction following radical anion formation, but there were no additional waves on the anodic sweep in the cyclic voltammograms that could be confidently ascribed to particular metal carbonyl fragments. The reduction potentials for the first electron are more negative than those for $RPCo_2Fe$ (possible fragmentation products), and they can be assigned to the couples $[RPFeCoMo]^{0,-}$. At room temperature in situ electrolysis of these clusters gave two single resonances in the ESR spectrum (g = 2.033) that may be Fe-based radicals.[27] For R = Me, an additional eight-line spectrum $\langle a \rangle$ = 6.0 mT was produced at 213 K (i.e., a monocobalt species) but only a broad band was displayed in the frozen solution spectrum. The large hyperfine coupling constant shows that the eight-line spectrum is not derived from a cluster moiety. On the other hand, PhPFeCoMo gave a well-resolved 15-line spectrum at low temperatures, $\langle g \rangle$ = 2.030 and $\langle a \rangle$ = −2.89 mT, that is probably due to $PhPCo_2Fe^-\cdot$.[26]

Current voltage curves of *t*-BuPFeCoNi in CH_2Cl_2 on Hg were characterized by a very complicated profile suggestive of rapid reaction or adsorption on Hg. On Pt, two irreversible electrode processes E_p^c = −0.33 and −0.75 V were discerned in CH_2Cl_2, but the scans were of poor quality due to rapid fouling of the electrode. In situ reduction at 213 K gave a highly asymmetric eight-line ESR spectrum, $\langle g \rangle$ = 2.049 and $\langle a \rangle$ = 2.21 mT, that could not be correlated with any known cobalt radical. Freezing of this solution gave a well-resolved spectrum, an analysis of which is compatible with more than one species being present. The most prominent features were assigned to the parallel set, $g_\parallel$ = 2.097 and $a_\parallel$ = −4.89 mT, with hyperfine coupling to one nucleus, spin 7/2; the other features were not identified. It seems unlikely from these parameters that the parallel features arise from a cluster radical anion.

Discussion

The series of clusters investigated in this paper allow an assessment of the influence of the capping and heterometal atoms on the redox properties of trinuclear clusters containing cobalt. It is evident from Table IV that both are important in establishing trends in the redox parameters, which in turn reflect changes in the energies and character of the upper bonding and LUMO levels.

Electron-Transfer Processes. Electron transfer in capped *homonuclear* trimetal carbonyl clusters follows the general pattern—a chemically and electrochemically reversible one-electron reduction step A separated ~0.7 V from a chemically irreversible reduction process at more negative potentials B. The diffusion currents of the two processes are often equal, and the second step in these cases can be ascribed to reduction to a short-lived dianion (eq 4). Nonintegral electron-transfer steps may also occur

$$ECo_3 \underset{A}{\overset{e}{\rightleftharpoons}} ECo_3^-\cdot \xrightarrow[B]{e} ECo_3^{2-} \xrightarrow{\text{fast}} \text{decomposition} \quad (4)$$

at the second reduction step, and in this case the process cannot be ascribed to the formation of a single entity such as a dianion and an ECE process can be recognized.[17]

It is interesting to note the electron-transfer sequence for these clusters, including the fact that the second wave in aprotic solvents is negative of the first wave by 0.7 V irrespective of the cluster, is very similar to that of aromatic hydrocarbons.[28] This highlights the analogy between a delocalized metal cluster with a singly degenerate antibonding LUMO and an aromatic moiety (which also has a singly degenerate LUMO). The modus vivendi for the nearly constant difference in the reduction potentials of the first and second electron-transfer steps is that both electrons are being added to a a_2^* LUMO, and, to a first approximation, the energy necessary to overcome electronic

(26) Beurich, H.; Madach, T.; Richter, F.; Vahrenkamp, H. *Angew. Chem., Int. Ed. Engl.* **1979**, *18*, 690.

(27) (a) Dawson, P. A.; Peake, B. M.; Robinson, B. H.; Simpson, J. *Inorg. Chem.* **1980**, *19*, 465. (b) Krusic, P. J.; San Filippo, J. Jr.; Hutchinson, B.; Hance, R. L.; Daniels, L. M. *J. Am. Chem. Soc.* **1981**, *103*, 2129.

(28) McKinney, T. M. *Electroanal. Chem.* **1980**, *10*, 97.

Table IV. Correlation of Spectroscopic and Electrochemical Data for Trimetal Clusters

cluster			$E_{1/2}$[a]	ν(CO),[b] cm^{-1}	λ_{max},[b] nm	$\langle a \rangle$,[c] mT
Me	C	Co_3	−0.58	2101	505	−3.66
Me	C	Co_2Cr	−0.76	2088	...	...
Me	C	Co_2Mo	−0.88	2086	578	−3.34
Me	C	Co_2W	−0.87	2075	564	...
Ph	C	Co_3	−0.56	2100	508	−3.58
Ph	C	Co_2Mo	−0.80	2086	597	−3.35
Ph	C	Co_2W	−0.85	2085	571	−3.59
Me	Ge	Co_3	−0.32	2108	530	−3.15
Me	Ge	Co_2Mo	−0.56	2080		−3.16
Ph	Ge	Co_3	−0.31	2090	529	−3.16
Ph	Ge	Co_2Mo	−0.60	2082		−3.04
Me	P	$FeCo_2$	−0.58	2093	553	−2.85
Me	P	FeCoMo	−1.13	2061	565	...
Ph	P	Co_3	0.45[d]	2095	695	−3.25
Ph	P	$FeCo_2$	−0.54	2101	545	−2.89
Ph	P	FeCoMo	−1.09	2067	...	...
Et_2N	P	$FeCo_2$	−0.59	2082	459	...
Et_2N	P	FeCoMo	−1.20	2050	525	...
t-Bu	P	$FeCo_2$	−0.57	2090	546	...
t-Bu	P	FeCoMo	−1.11	2063	563	...
t-Bu	P	FeCoNi	−1.15	2063	564	...

[a] V. vs. Ag/AgCl for [compound]$^{0,-}$ in CH_2Cl_2. [b] In hexane for neutral cluster, the shift from hexane to CH_2Cl_2 is significant. [c] In CH_2Cl_2 for radical anion. [d] Refers to couple $[PhPCo_3]^{+,0}$.

charge repulsion (~70 kJ mol^{-1}) on the addition of the second electron will be independent of metal composition.

The incorporation of a heteroatom into the trinuclear framework increases the kinetic lability of the reduced species and has a marked effect on the sequence of reversible/irreversible steps. $RGeCo_2Mo$ and $RPCo_2Fe$ clusters can be considered together. In both cases the sequence follows that given for ECo_3 (eq 1) and the first reduction process (A) is unaffected by CO or temperature.[29] If the CV scans are switched just past E_p^c(A) there is no evidence for the formation of $Co(CO)_4^-$; this only appears after E_p^c(B). There is no doubt the first reduction process corresponds to the formation of the radical anions $RGeCo_2Mo^{-\cdot}$/$RPCo_2Fe^{-\cdot}$, and this assignment is supported by the ESR data (vide infra). There is a much smaller separation between $E_{1/2}$(A) and $E_{1/2}$(B) with these clusters compared to that for ECo_3. In terms of the explanation given above the electronic charge repulsion term may be smaller in the heteronuclear cluster (the ν(CO) data indicate that the charge density on the cobalt atoms is smaller) but, equally well, the kinetic parameters associated with the ECE process for B could cause this trend.

The incorporation of a second heterometal into the cluster gives reduced species that rapidly fragment by metal–metal bond cleavage; the lifetime of species such as $RPFeCoNi^{-\cdot}$ and $RPFeCoMo^{-\cdot}$ is estimated to be less than 1 ms. Consequently, no well-defined second reduction step was seen in electrochemical scans of these species (eq 5).

$$RPCoMM' + e \xrightarrow[A]{e} [RPCoMM']^{-\cdot} \xrightarrow{fast} \text{decomposition} \quad (5)$$

An interpretation of the data for the carbon-capped *heterometal* clusters $RCCo_2M$ is not so straightforward. For these clusters the sequence of reversible/irreversible steps found in the other capped clusters is reversed. We shall denote the first and second reduction steps as C and D, respectively, since neither the structural species nor the electrokinetic processes may be the same as those for A and B described above. The pertinent results for a mechanistic interpretation can be summarized as follows.

(a) Overall the two reduction steps correspond to a two-electron transfer and, under conditions where C has chemical reversibility, have the characteristics of one-electron transfers. Where ECCE processes become significant, there is an increase in the limiting current of C at the expense of *D*.

(b) The electrochemical responses shown by C are independent of the production of the reduced species associated with D as CV scans switched before D are the same as those switched after D. C must therefore be associated with the formation of the radical anions $RCCo_2M^{-\cdot}$ arising directly from $RCCo_2M$.

(c) D is chemically and electrochemically reversible, and its potential is nearly invariant under all conditions. For a given apical substituent (i.e., R = Me or Ph) $E_{1/2}^r$ is practically independent of the heterometal M, which suggests that the second electron has entered an orbital centered on the cobalt framework.

(d) C is a kinetically controlled reduction process, and the potential (E_p^c), cathodic, and anodic diffusion or peak currents are a function of scan rate, [CO], and temperature (Table III). With all clusters C becomes more chemically reversible at low temperatures and at very fast scan rates. The same holds for the effect of CO for $RCCo_2M$ (M = Mo, W), but CO has little effect on the chemical reversibility of the $RCCo_2Cr$ system.

(e) The behavior of C is characteristic of an ECE process and, certainly for $RCCo_2Cr$, an ECCE process in which at least two coupled chemical reactions are involved. Some of the data could be consistent with a CE component, but there was no evidence for a prior chemical step (such as metal–metal bond cleavage) for $RCCo_2M$ (M = Mo, W).

(f) $RCCo_3(CO)_9^{-\cdot}$ is identified as a dominant decomposition product for the $RCCo_2Cr$ system (especially under CO), and it can also be identified in the $RCCo_2W$/CO system.[30]

(29) That is, the electrochemical and chemical reversibility does not change in the presence of CO temperature down to 213 K.

(30) It should be noted that the companion reduction wave for $RCCo_3(CO)_9$ is not seen on the scan following oxidation of $RCCo_3(CO)_9^{-\cdot}$. This means that the radical anion is involved in a further rapid reaction that is not unreasonable as it is activated to nucleophilic attack.[7,31] The nucleophile could be $CpM(CO)_3^-$ which would lead to regeneration of the parent radical anion $RCCo_2M(CO)_8Cp^{-\cdot}$.[32]

(31) Brezems, G. J.; Rieger, P. H.; Visco, S. J. *J. Chem. Soc., Chem. Commun.* **1981**, 265.

(32) Jensen, S.; Robinson, B. H.; Simpson, J. *J. Chem. Soc., Chem. Commun.* **1983**, 1081.

Scheme I

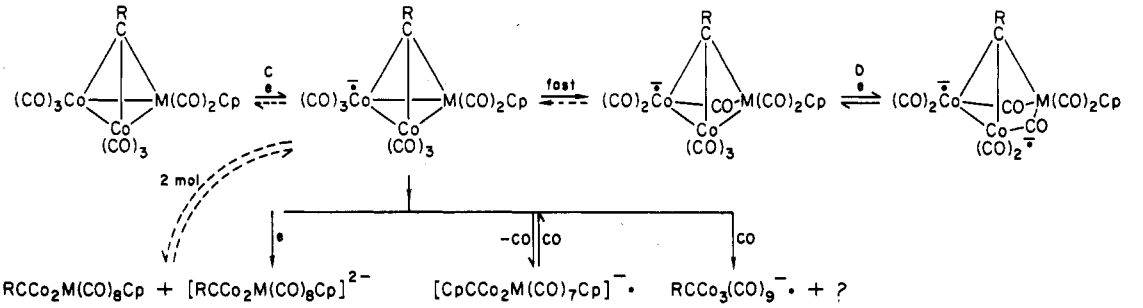

(g) Because of the kinetic control trends in the reduction potentials of C must be interpreted with caution. Nonetheless, at the same temperature and in the same solvent under nitrogen, the peak separation E_p^{red} (C–D) decreases in order Cr > W ≈ Mo and there is a dependence on the apical substituent. This suggests that both the heterometal fragment $M(CO)_2Cp$ and the carbyne cap are still structural entities associated with C.

(h) Polar solvents such as THF stabilize the anionic species associated with C. The kinetic stability of these species increases in order Cr < W < Mo; the $RCCo_2Mo$ system provides the most chemically reversible system.

$RCCo_2M$ clusters are chemically more reactive than their homonuclear counterparts; $RCCo_2Cr$ clusters are extremely labile.[11,14,33] Metal–metal cleavage reactions are well-known,[34] and the metal–metal bonds are subordinate to the capping carbyne–metal interaction in confering kinetic and thermodynamic stability upon the cluster. Clearly the radical anions $[RCCo_2M]^{-}\cdot$ are even more labile, but the electrochemical lability follows the same order as the chemical lability of the neutral species. Given these data we conclude that an intimate structural interpretation of the complex electrochemical responses is not possible but a feasible reaction scheme is given in Scheme I. What is certain is that the species associated with D is *not* isostructural with the parent clusters or radical anions and that the $M(CO)_2Cp$ site is electron-rich and unlikely to be reversibly reduced.[39] In the scheme formation of the radical anion induces rapid "opening" of the cluster, a process more likely to occur without subsequent fragmentation when the group 6 metal is Mo. Reduction of the "open" clusters produces a diamagnetic species. This accounts for the absence of a long-lived paramagnetic species in the ESR spectra and that D is not CO dependent. The monocobalt paramagnetic species found at ~213 K (see Table II) may be the paramagnetic precursor to D.

Radical anions retaining the usual capped "closed" structure are only found in the ESR spectra under conditions where C has chemical reversibility and are absent for the labile chromium species. Several possibilities exist for the coupled reactions that accompany radical anion formation. There are clearly two CO-dependent reactions, one which restricts the chemical reversibility of C via CO dissociation from the radical anion and the other which produces $RCCo_3(CO)_9^{-}\cdot$ as a decomposition product. Where the limiting current for C in the dc polarograms is enhanced compared to D (the situation with $RCCo_2Cr$), a disproportionation reaction can be invoked, providing the reduction step corresponding to dianion formation is "hidden" underneath the reversible wave D (eq 6). This

$$RCCo_2M \rightleftharpoons RCCo_2M^{-}\cdot \xrightarrow{e} RCCo_2M^{2-} \xrightarrow{RCCo_2M} 2RCCo_2M^{-}\cdot \quad (6)$$

is not unreasonable as the second reduction step for $RGeCo_2M$ clusters is separated by only 0.3 V from the first. Conversely, conproportionation[17] may be rapid (especially for $RCCo_2Mo$) which could account for the oxidation wave of $RCCo_2Mo^{-}\cdot$ seen at low temperatures with no companion reduction component (Figure 8d).

ESR Parameters of Cluster Radical Anions. Radical anions of $RECo_3$ and $RECo_2M$ clusters apart from $RCCo_2Cr^{-}\cdot$ were characterized, and the data are given in Table II. In common with most cluster radical anions[5] electron delocalization reduces spin–orbit coupling and the **g** tensor anisotropy is small. It is noticeable that the isotropic and anisotropic **g** tensors are closer to the free-electron value for the carbon-capped clusters. This may be due to the greater involvement of the carbyne p_π orbitals in the cluster bonding[41] than the p_π orbitals of the heavier capping groups like Ge, although in the homonuclear clusters the electron is in an orbital with no capping group character.

The especial position of carbon-capped clusters is also seen in their larger isotropic hyperfine coupling constants, $\langle a \rangle_{Co}$, both for the homonuclear and heteronuclear species. The order of decreasing $\langle a \rangle_{Co}$ is RC ≈ S > RP > RGe (homonuclear) and RC ≈ S > RGe > RP (heteronuclear). Isotropic cobalt coupling is the sum of a number of contributions from polarization of the inner shell s orbitals and from admixture of 4s character into the MO containing the unpaired electron (zero admixture for clusters of C_{3v} symmetry). Symmetry arguments developed earlier[4,6a]

(33) (a) Vahrenkamp, H. *Adv. Organomet. Chem.*, in press. (b) Vahrenkamp, H. *Angew Chem., Int. Ed. Engl.* **1978**, *17*, 379.

(34) Interconversions involving metal–metal cleavage in capped systems during which the cluster retain its rigidity are usually brought about by the addition or elimination of nucleophiles.[35-37] The addition of an electron or electrons to the metal framework is essentially similar to nucleophilic attack as it is the increased charge density on the cluster which initiates metal–metal bond opening. Examples without capping groups holding the cluster together are known with the heavier transition elements.[38]

(35) Vahrenkamp, H. *Philos. Trans. R. Soc. London* **1982**, *308*, 17.

(36) (a) Huttner, G.; Schneider, J.; Müller, H. D.; Mohr. G.; von Seyerl, J.; Wohlfahrt, L. *Angew. Chem., Int. Ed. Engl.* **1979**, *18*, 76. (b) Schneider, J.; Zsolnai, L.; Huttner, G. *Chem. Ber.* **1982**, *115*, 989.

(37) Richter, F.; Vahrenkamp, H. *Organometallics* **1982**, *1*, 756.

(38) Deeming, A. J.; Johnson, B. F. G.; Lewis, J. *J. Chem. Soc. A* **1970**, 897.

(39) We have considered the possibility that $Cp_2M_2(CO)_6$ or derived species are responsible for some of the electrochemical behavior, but this was rejected. The dimers M = Mo and W undergo an irreversible two-electron reduction, but a comparable reduction is not seen for $Cp_2Cr_2(CO)_6$; the potentials are in between those for C and D.[40] We could not detect the dimers (IR, TLC) before or after reduction. More likely candidates are $CpM(CO)_3^{-}$ or $CpM(CO)_3\cdot$. Again, the potentials for their irreversible reduction do not correspond to C or D or other prominent waves at negative potentials, and there were no reversible oxidation waves expected for $CpM(CO)_3^{-}$.[40]

(40) Madach, T.; Vahrenkamp, H. *Z. Naturforsch. B: Anorg. Chem., Org. Chem.* **1979**, *34B*, 1195.

(41) Kostic, N. M.; Fenske, R. F. *J. Am. Chem. Soc.* **1981**, *103*, 4677.

Scheme II

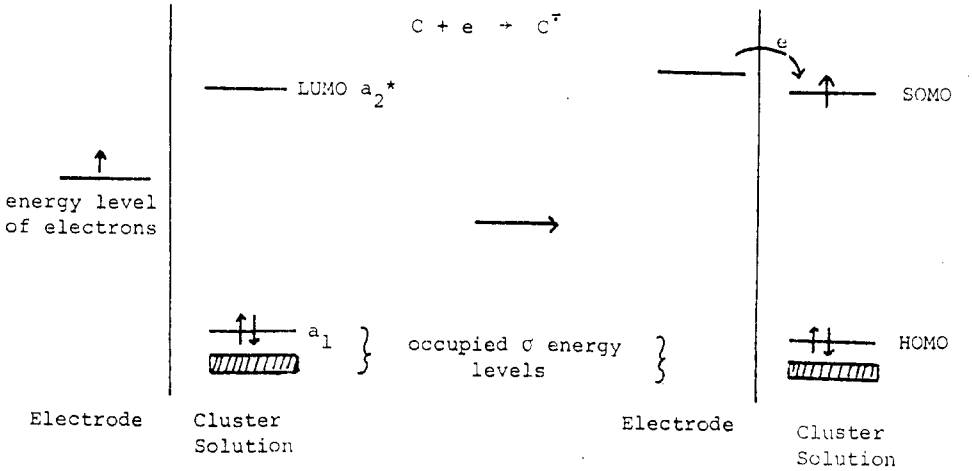

define the orbital containing the unpaired electron in the C_{3v} clusters $RCCo_3$, $RGeCo_3$, and $RPCo_3$ as an a_2* orbital, primarily cobalt $3d_{xy}$. This is confirmed by the negative dipolar hyperfine tensor $\mathbf{b}_{\parallel}$ and an estimate of the cobalt 3d spin density (ρ) can be obtained from this parameter by using the relationship[42] $\mathbf{b}_{\parallel} = -^4/_7 P\rho^{3d}$. It is considerably lower for $RGeCo_3^{-}\cdot$ (~60%) than either $RCCo_3^{-}\cdot$ or $RPCo_3^{-}\cdot$ (~75%), and we speculate that the (presumably) different orbital character arises from the greater strain (with respect to cap–Co_3 overlap) in the germanium compounds.[43] A comparable assessment for the heteronuclear clusters is more difficult because the C_s symmetry does not uniquely define the orbital composition, and the anisotropic ESR parameters are a function of the angle relating the principal axes of the hyperfine tensors.[4] A detailed analysis will be presented elsewhere,[19] but qualitatively the hyperfine tensors suggest that by far the greater proportion of spin density resides on the cobalt atoms. It is also significant that the differences in $\langle a \rangle_{Co}$ between $RCCo_2M^{-}\cdot$, $RGeCo_2M^{-}\cdot$, and $RPCo_2M^{-}\cdot$ are actually the result of smaller $a_{\perp}$ for the latter two species since $a_{\parallel}$ is very similar.

Correlation of Reduction Potentials with Spectral Data. Reduction potentials for the couples $[RECo_3]^{0,-}$ and $[RECo_2M]^{0,-}$ are summarized in Table IV. We recognize that any comparison utilizing the irreversible electron-transfer steps of $[RCCo_2M]$ is difficult. Nevertheless, two important trends in the data can be discerned. (a) It is easier to reduce germanium-capped clusters than the carbon-capped analogues and $E_{1/2}{}^{r}[RGeCo_2Mo]^{0,-} \approx [RPCo_2Fe]^{0,-}$. (b) It is more difficult to reduce the heterometal species $RECo_2M$. A simple picture of the reduction process which enables trends in reduction potentials (i.e., free energies) to be correlated with changes in the LUMO energy relative to the hypothetical electrode orbital energy is shown in Scheme II.[44]

It is convenient to consider the isostructural homonuclear clusters first where the ligand conformation remains constant. From Scheme II the lower reduction potential for $RGeCo_3$ suggests that the LUMO of $RGeCo_3$ is lower in energy than in $RCCo_3$. While the capping atom cannot directly perturb the a_2* orbital as it has no capping atom character, its energy relative to the σ-bonding levels (and hence HOMO) will be influenced by the Co–Co σ-bonding interactions for which the appropriate orbitals are indeed

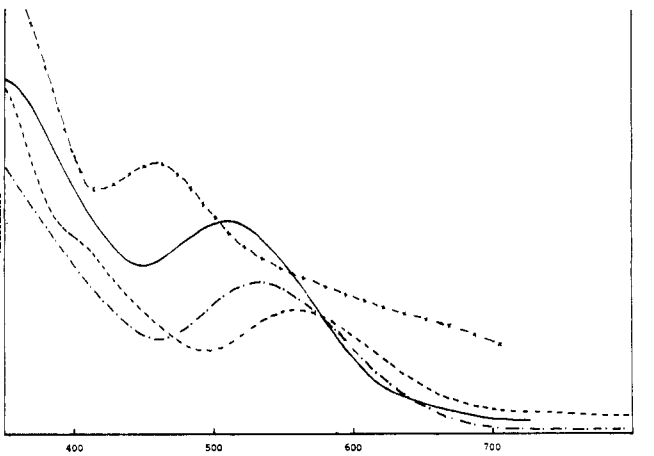

Figure 13. Visible spectra in CH_2Cl_2 at 298 K: —, $MeCCo_3(CO)_9$; - · -, $MeGeCo_3(CO)_9$; - - -, $MeCCo_2W(CO)_8Cp$; -×-, $Et_2NPCo_2Fe(CO)_9$.

"cluster" orbitals.[6b,45] $RGeCo_3$ is more strained than $RCCo_3$ because of the larger covalent radius of Ge;[43] the Ge–Co overlap is more "bent". These structural constraints will not drastically affect the a_2* LUMO but they will perturb the energy of the bonding "cluster" orbitals. The trend in $E_{1/2}$, C < Ge, is therefore primarily the result of decreased electron density in σ-bonding orbitals with a Co–Co component, which indirectly lowers the LUMO energy.

Photoelectron spectra of $RGeCo_3$ would confirm this point, but we have shown[46] that visible spectra of capped metal carbonyl clusters can give valuable information on the separation between the upper bonding levels and the LUMO. Data from these spectra should therefore complement the deductions on HOMO–LUMO separations from the electrochemical data. Tricobalt carbon clusters characteristically have two absorption bands in their visible spectra.[46,47] The band of lowest energy at ~510 nm is a broad multicomponent transition from the upper σ-bonding orbitals to the LUMO; the σ(HOMO) → σ* transition is only resolved at low temperatures as a shoulder on the low-energy side of this band. The second band ~370 nm, of comparable extinction coefficient to the first, involves transitions from the π levels to the LUMO.

(42) Morton, J. R.; Preston, K. F. *J. Magn. Reson.* **1978**, *30*, 577.
(43) Schmid, G. *Angew. Chem., Int. Ed. Engl.* **1978**, *17*, 392.
(44) For the reversible diffusion-controlled electron transfer $E_{1/2}{}^{r} \approx E_0$. To a first approximation one free energy term $\Delta G_{electrode}$, the electrode orbital energy, is fixed so relative changes in $E_{1/2}{}^{r}$ reflect the relative position of one free energy term, the LUMO energy.
(45) Several photoelectron studies have appeared recently, e.g.: (a) Chesky, P. T.; Hall, M. B. *Inorg. Chem.* **1981**, *20*, 4419. (b) Xiang, S. F.; Bakke, A. A.; Chen, H.-W.; Eyermann, C. J.; Hoskins, J. L.; Lee, T. H.; Seyferth, D.; Withers, H. P.; Jolly, W. L. *Organometallics* **1982**, *1*, 699.
(46) (a) Colbran, S.; Robinson, B. H.; Simpson, J. *Organometallics* **1983**, *2*, 952. (b) Colbran, S.; Hanton, L.; Robinson, B. H.; Simpson, J. *J. Organomet. Chem.*, manuscript submitted.
(47) Geoffroy, G. L.; Epstein, R. A. *Inorg. Chem.* **1977**, *16*, 2795.

Scheme III

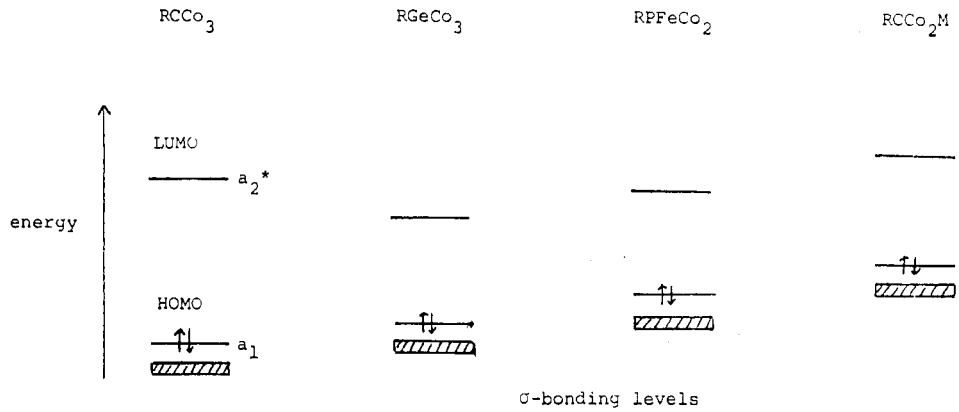

Consequently, the low-energy band in the electronic spectra of the capped clusters could correlate with the electrochemical data; the data are summarized in Table IV. As shown by Figure 13, the $RGeCo_3$ clusters have the same spectral profile as $RCCo_3$ but with a red shift of the low-energy band. This red shift of $\sim$1000 cm^{-1} substantiates the argument that the σ-bonding LUMO separation is smaller in $RGeCo_3$.

Let us see if this correlation extends to the heteronuclear clusters. Indeed the profile of the visible spectra of all capped trinuclear clusters is remarkably similar to $RCCo_3$ which gives some confidence in the generality of the assignments discussed above. The reduction potentials for $RPFeCo_2$ and $RCCo_3$ (R = Ph, Me) are virtually the same, but there is a red shift in the electronic absorption band of $RPFeCo_2$ of some 1500 cm^{-1}. This indicates that there is a relative decrease in the σ-bonding LUMO separation, but since there is an equality in $E_{1/2}^{r}$, this must arise from an increase in the energy of the σ-bonding orbitals relative to $RCCo_3$. The orbital energies of $RPFeCo_2$ are thus in contradistinction to those of $RGeCo_3$ (see Scheme III below).

The trend in E_p^{red}, $[RECo_3]^{0,-}$ > $[RECo_2M]^{0,-}$ and $[RPCo_2Fe]^{0,-}$ < $[RPCoFeM]^{0,-}$ is a direct consequence of replacing an electronegative group $Co(CO)_3$ by an electron-rich moiety $M(Cp)(CO)_2$. In the carbon-capped series this is accompanied by a large red shift (Figure 12, Table IV) and in fact the *smallest separation* between the σ-bonding levels and the LUMO occurs with these clusters *even though they are the most difficult of the $RECo_2M$ clusters to reduce.*[48] This particular example illustrates the danger in interpreting trends in electrochemical data simply in terms of a HOMO–LUMO separation. As the orbital sequence in Scheme III shows, there is an overall increase in orbital energy which makes reduction more difficult, but the HOMO–LUMO separation decreases relative to $RCCo_3$. This is reasonable as extra electronic charge is being placed on the cluster by the $M(Cp)(CO)_2$ moiety. We speculate that the higher energy of the LUMO (and therefore the SOMO) in the $RCCo_2M$ clusters encourages the "opening" of the cluster upon reduction with consequential changes in the accessible electrode processes (vide supra) and the greater kinetic and thermodynamic instability which is seen in their reaction chemistry. Again, in the P-capped series, the progressive red shift on replacing a $Co(CO)_3$ unit by $M(Cp)(CO)_2$ continues to RPCoFeMo (Table IV) although it is not as marked as in the C-capped series. The anomalous derivatives are $Et_2NPFeCo_2$ and $Et_2NPFeCoMo$. Whereas the E_p^{red} values follow the general trends, the visible bands are some 50 nm lower than expected (Figure 12). Clearly it is due to a special feature of Et_2N, a group which can participate in mesomeric interactions with the cluster.[45,49] Whether these interactions have changed the order of the bonding levels, or the observed band is not that involving the σ levels but rather the band arising from π-level transitions shifted from its normal position around 400 nm, with consequential loss of the first band in the low energy tail, cannot be decided without UPE data.

Scheme III summarizes the qualitative orbital relationship for neutral capped trinuclear clusters as determined from this combined electrochemical/visible spectra approach.

The second band in the visible spectra that involves the π-bonding levels does not change significantly from homo- to heteronuclear clusters with the same capping group, as expected if the spectral assignment is correct. There are small changes with capping group in order of energy: RC > RP $\approx$ RGe.

The changes in electron density that are mirrored in the electrochemical and spectral data may not necessarily be obvious in the ν(CO) or $\langle a \rangle_{Co}$ data, as the former is a ground-state parameter, whereas the latter reflects the spin distribution in the SOMO. For trinuclear clusters the ν(CO) totally symmetric A_1 mode is a sensitive probe of electron density on the cluster,[50] and, as expected, the energy of this band decreases when the cluster incorporates an electron-rich $M(Cp)(CO)_2$ unit. On the other hand, data points on plots of reduction potential against ν(CO) are widely scattered and there is no direct relationship between them except that the increase in electron density on the cluster makes the reduction potential more negative in conjunction with the decrease in ν(CO). The influence of the capping group is seen in the much larger perturbations in the data with an RP instead of an RC group. This is attributed to the inability of the P atom to participate in the π interactions that allow the tricobalt carbon cluster to participate in "push–pull" electronic interactions that buffer changes in electronic charge. The anomalous position of Me_2N clusters is again seen in the lower energy of ν(CO) in Me_2NPCo_2Fe and $Me_2NPCoFeMo$, consistent with the Me_2N group acting as a net π donor. Hyperfine coupling constants $\langle a_{Co} \rangle$ are determined by the spin density rather than the charge density, and it is not surprising that there is no correlation between $\langle a_{Co} \rangle$ and E_p^{red} or ν(CO) over the series of clusters investigated herein. The changes in spin density reflect an alteration to the orbital character of the a_2* level as discussed above (vide supra).

(48) This argument holds irrespective of the effect of the coupled chemical reactions.

(49) Seyferth, D. *Adv. Organomet. Chem.* **1976**, *14*, 97.
(50) Penfold, B. R.; Robinson, B. H. *Acc. Chem. Res.* **1973**, *6*, 73.

Conclusion

Capped trimetal clusters are readily reduced to the corresponding radical anions, but the subsequent electrochemical, kinetic and chemical behavior of the anions depends on the metal composition. Despite the complex electron-transfer processes in some cases this work shows that considerable information on the electronic structure of metal clusters can be obtained from studies of their electron-transfer properties coupled with other spectroscopic data. Further papers will extend this concept to clusters of higher nuclearity.

Acknowledgment is made to the donors of the Petroleum Research Fund, administered by the American Chemical Society, for partial support of this research. H.V. also thanks the Deutsche Forschungsgeminschaft for support of research at Freiburg and Otago. We are also grateful for assistance from the University of Otago for the visits to Dunedin of H.V. and A.M.B.

Registry No. $MeCCo_3(CO)_9$, 13682-04-7; $PhCCo_3(CO)_9$, 13682-03-6; $MeGeCo_3(CO)_9$, 70686-34-9; $PhGeCo_3(CO)_9$, 29998-27-4; $MeCCo_2Cr(CO)_8Cp$, 68185-41-1; $PhCCo_2Cr(CO)_8Cp$, 68185-44-4; $MeCCo_2Mo(CO)_8Cp$, 68185-42-2; $PhCCo_2Mo(CO)_8Cp$, 68185-45-5; $MeCCo_2W(CO)_8Cp$, 68185-43-3; $PhCCo_2W(CO)_8Cp$, 68185-46-6; $MeGeCo_2Mo(CO)_8Cp$, 78793-63-2; $PhGeCo_2Mo(CO)_8Cp$, 78793-62-1; $MePCo_2Fe(CO)_9$, 87160-19-8; $PhPCo_2Fe(CO)_9$, 69569-55-7; $BuPCo_2Fe(CO)_9$, 88131-01-5; $Et_2NPCo_2Fe(CO)_9$, 88131-02-6; $MePCoFeMo(CO)_8Cp$, 87526-93-0; $PhPCoFeMo(CO)_8Cp$, 69569-57-9; *t*-$BuPCoFeMo(CO)_8Cp$, 87526-94-1; *t*-$BuPCoFeNi(CO)_6Cp$, 87527-00-2; $PhPCo_3(CO)_9$, 57143-38-1; $[MeCCo_3(CO)_9]^-$, 61024-79-1; $[PhCCo_3(CO)_9]$, 61024-80-4; $[MeGeCo_3(CO)_9]^-$, 88131-03-7; $[PhGeCo_3(CO)_9]^-$, 88131-04-8; $[MeCCo_2Mo(CO)_8Cp]^-$, 88131-05-9; $[PhCCo_2Mo(CO)_8Cp]^-$, 88131-06-0; $[PhCCo_2W(CO)_8Cp]^-$, 88131-07-1; $[MeGeCo_2Mo(CO)_8Cp]^-$, 88131-08-2; $[PhGeCo_2Mo(CO)_8Cp]^-$, 88131-09-3; $[MePCo_2Fe(CO)_9]^-$, 88131-10-6; $[PhPCo_2Fe(CO)_9]^-$, 71393-16-3; $[PhPCo_3(CO)_9]$, 88156-65-4; $[SCo_2Fe(CO)_9]^-$, 77845-72-8; $[PhCCo_2Cr(CO)_8Cp]^-$, 88131-11-7; $[PhPCoFeMo(CO)_8Cp]^-$, 88131-12-8; $[MePCoFeMo(CO)_8Cp]^-$, 88131-13-9; [*t*-$BuPCoFeNi(CO)_6Cp]^-$, 88156-66-5.

^{119}Sn NMR Spectroscopic Studies of Organotin Phosphates as Catalysts for the Polymerization of Epoxides

Junzo Otera,*[1a] Toru Yano,[1a] Etsuko Kunimoto,[1a] and Tetsuya Nakata[1b]

Okayama University of Science, Ridai-cho, Okayama 700, Japan, and Research Laboratories, Osaka Soda Co., Ltd., 9 Otakasucho, Amagasaki 660, Japan

Received August 9, 1983

Various organotin phosphates and pyrophosphates were prepared as model compounds for organotin phosphate catalysts effective for polymerization of epoxides. Pyrolysis of the butyltin compounds thus obtained was conducted with the pure compounds or in the presence of dibutyl phosphate (DBP). ^{119}Sn NMR spectra allowed the characterization of these compounds. It was found that phosphato ligands are easily condensed to give P–O–P linkages and that DBP cleaves Sn–C bonds. Quite interestingly, however, the last butyl group attached to the tin resisted cleavage, and thus monobutyltin compounds resulted as final products in all cases. When an excess of DBP was present, condensation of this compound with pyrophosphato ligands took place. Condensates prepared from di- or tributyltin chlorides and oxides with tributyl phosphate under various reaction conditions also were characterized on the basis of ^{119}Sn NMR spectra. In every case, it was found that the final products are analogous to those derived from model compounds. Polymerization studies of epichlorohydrin by various organotin phosphates and pyrophosphates as model compounds led to the conclusion that the monobutyltin pyrophosphate **11** is associated with an actual active species. On the basis of these results, the nature of organotin phosphate catalysts is discussed.

Introduction

It has been found that condensates obtained by treating organotin halides or oxides with trialkyl phosphates at about 250 °C are highly active catalysts that afford high molecular weight polymers from epoxides.[2] That organotin derivatives show such a high catalytic activity seems quite surprising since the most commonly used catalysts are derived from more acidic metals such as aluminum[3] and zinc.[4] In addition, organotin phosphate catalysts have a practical advantage over organoaluminum and -zinc catalysts in that they can be handled in air. Another feature of organotin catalysts is that they afford polymers of high crystallinity, indicating that the polymerization proceeds highly stereospecifically. Therefore, it appeared to us of great interest to investigate the nature of these catalysts. Since they are presumed to be pyrolysis products of organotin phosphates, preparation and pyrolysis of authentic organotin phosphates would provide useful information. Thus far, studies on organotin phosphates have been rather limited. Ridenour et al. have investigated some di- and triorganotin dialkyl phosphates.[5] More recently, Zuckerman and his co-workers have reported the preparation and characterization of di- and triorganotin diphenyl phosphates.[6]

At the outset of our studies on organotin phosphate catalysts, we prepared various organotin phosphates and pyrophosphates. The pyrolysis products of these compounds were investigated by means of ^{119}Sn NMR spectra in the hope of elucidating the species involved and also the reaction mechanism of pyrolysis.

Moreover, on the basis of these results, condensates prepared from di- or tributyltin chlorides and oxides were

(1) (a) Okayama University of Science. (b) Osaka Soda Co., Ltd.
(2) Nakata, T. "Coordination Polymerization"; Price, C. C., Vandenberg, E. J., Eds.; Plenum Press: New York, 1983; p 55.
(3) Vandenberg, E. J. *J. Polym. Sci.* **1960**, *47*, 486.
(4) Furukawa, J.; Tsuruta, T.; Sakata, R.; Saegusa, T. *Makromol. Chem.* **1959**, *32*, 90.
(5) Ridenour, R. E.; Flagg, E. E. *J. Organomet. Chem.* **1969**, *16*, 393.
(6) Molloy, K. C.; Nasser, F. A. K.; Zuckerman, J. J. *Inorg. Chem.* **1982**, *21*, 1711.

0276-7333/84/2303-0426$01.50/0